Acta Materialia 115 (2016) 1–9

Contents lists available at ScienceDirect

Acta Materialia

journal homepage: www.elsevier.com/locate/actamat

Full length article

Twin boundary activated α → ω phase transformation in titanium under shock compression

Hongxiang Zong [a, b, *], Xiangdong Ding [a, **], Turab Lookman [b], Jun Sun [a]

[a] State Key Laboratory for Mechanical Behavior of Materials, Xi'an Jiaotong University, Xi'an 710049, China
[b] Theoretical Division, Los Alamos National Laboratory, Los Alamos, NM 87545, USA

ARTICLE INFO

Article history:
Received 26 February 2016
Received in revised form
20 May 2016
Accepted 24 May 2016
Available online 31 May 2016

Keywords:
Deformation twinning
Martensitic transformation
Shock compression
Titanium

ABSTRACT

The role of grain boundary structures on the shock response of hexagonal-close-packed (hcp) metals is little understood. We use molecular dynamics simulations to investigate deformation mechanisms in shock compressed Ti bicrystals with three types of grain boundary (GB) microstructure. Our results show the shock response of phase Ti polycrystals are influenced by the GB characteristics, i.e., elastic shock wave induced inelastic deformation occurs on both sides of the $\{10\bar{1}2\}$ coherent twin boundaries (CTBs) but only on one-side of the symmetric incoherent twin boundaries (ITB) or $\{1\bar{2}10\}$ tilt grain boundaries regions. In particular, we find that the elastic shock wave can readily trigger the $\alpha \rightarrow \omega$ transformation at $\{10\bar{1}2\}$ CTBs but not the other two GBs, and the $\alpha \rightarrow \omega$ transformation at CTBs leads to considerable wave attenuation (i.e., the elastic precursor decay). Combined with first principle calculations, we find that CTBs can facilitate the overcoming of the energy barrier for the $\alpha \rightarrow \omega$ transformation. Our findings have the potential to influence interface engineering and materials design under extreme conditions.

1. Introduction

Improving our understanding and predictive capability of shock-loaded materials requires understanding the complex interaction of shocks with the material microstructure. It is well known that microstructure affects the response of a material to dynamic loading as dislocations, stack faults, grain boundaries (GBs) and other heterogeneities can act as defect sites that can promote plastic deformation and phase transformation [1–5]. The behavior of GBs under dynamic mechanical loads is of particular interest as it impacts the bulk properties of polycrystal materials in many respects [2,6,7]. In particular, when the grain size is reduced to ultrafine or nano-scale, the effects of GBs on the material properties become more significant since the traditional deformation mechanisms based on nucleation and propagation of dislocations are replaced gradually by GB mediated processes, such as GB sliding [8,9], grain rotation [10,11], dislocation nucleation or absorption at GBs etc [2,12]. Therefore, the influence of GBs needs to be considered in detail in understanding and modeling the shock response of materials (broadly defined to include plastic deformation and phase transformation).

In previous experimental and numerical work, plastic deformation and phase transition under shock compression have been routinely studied in polycrystalline solids via experiments [13,14] and nano-polycrstalline solids using molecular-dynamics (MD) simulations [6,15,16]. Recent experimental work by Kanel et al. indicate that the onset of stress for dynamic fracture (i.e. spall strength) of single-crystal Cu is more than twice that of polycrystalline Cu [17], which suggests that the threshold stress for nucleation of voids at a GB might be significantly lower than for homogeneous nucleation. Germann et al. point out from simulations of the $\alpha - \varepsilon$ martensitic transformation in Fe nanocrystals that grain boundaries play an important role in determining the shock wave profiles and phase transformation kinetics [15]. It has also been shown that grain boundaries can change the coupling between plasticity and phase transformation, resulting in different phase transformation mechanisms [6]. However, it is still unclear what the role of the atomic structure of GBs on the dislocation glide or phase transformation processes, particularly in low symmetry crystal metals even though recent experiments have further stressed the importance of GBs during shock wave loading [18–20].

Given the vast number of GB types and grain characteristics, it is

* Corresponding author. State Key Laboratory for Mechanical Behavior of Materials, Xi'an Jiaotong University, Xi'an 710049, China.
** Corresponding author.
E-mail addresses: zonghust@mail.xjtu.edu.cn (H. Zong), Dingxd@mail.xjtu.edu.cn (X. Ding).

http://dx.doi.org/10.1016/j.actamat.2016.05.037
1359-6454/

highly desirable to investigate some elemental processes, such as bicrystals, to gain specific insight without being overwhelmed by the complexities of abundant random GBs. The role of the GB structure on mechanical response has been widely discussed in bicrystals under quasi-static loading conditions [21,22]. The deformation mechanisms at GBs have been found to depend upon not only the misorientation between grains but also the GB plane inclination [9,23,24]. Besides the commonly observed tilt grain boundaries, several special GB structures have attracted considerable attention since they often form during fabrication and play a crucial role in determining mechanical performance. For example, symmetric $\sum 3\{111\}$ GBs or coherent twin boundaries (CTBs) in Cu exhibit a superior combination of ultrahigh strength, good ductility and high fatigue resistance, compared to other GB structures [25,26]. Our previous studies on 90° GB or incoherent twin boundaries (ITBs) in Ti demonstrate that the deformation mechanisms of ITBs is dominated by a uniaxial stress coupled GB migration [23].

In this study, we investigate the shock response of Ti bicrystals with three different GB geometries (i.e., CTB, ITB as well as tilt GB) by a combination of MD simulations and first principle calculations. Our results indicate that the dislocation activity and the $\alpha \rightarrow \omega$ phase transformation kinetics in shock-loaded Ti depend on GB structures. In particular, a $\{10\bar{1}2\}$ CTB activated $\alpha \rightarrow \omega$ transformation is observed. The outline of the paper is as follows. We describe in Section 2 the atomic simulation methodology. In Sections 3 and 4, we choose models of Ti bicrystals containing three types of GB structures to study the interaction of shock waves with these GBs. We investigate the corresponding deformation mechanisms at the GBs and clarify the underlying mechanisms for the GB structure dependent $\alpha \rightarrow \omega$ transformation processes. Finally, the main results and conclusions are summarized in Section 5.

2. Methodology

The molecular dynamics (MD) simulations were carried out using the Large-scale Atomic/Molecular Massively Parallel Simulator (LAMMPS) code [27]. Up to about 3.0 millions atoms were used to ensure that the simulations were adequate to cover both the atomistic details and the phase transformation microstructure. The initial Ti bicrystal samples (the GB normals are defined as the z-axis) with dimensions $Lx = 17.3$ nm, $Ly = 17.3$ nm, and $Lz = 112.4$ nm were constructed by using the coincidence site lattice method. In our simulations, three types of samples (i.e., sample A, B and C) are employed, and the orientations of the grains are given in Fig. 1. Specifically, the crystallographic orientations of two grains within sample A are $(10\bar{1}2)_{Grain2}//(\bar{1}01\bar{2})_{Grain2}$ and $[10\bar{1}0]_{Grain1}//[\bar{1}010]_{Grain2}$, similar to $\{10\bar{1}2\}$ CTBs. Sample B has the same crystallographic orientations as ITBs reported in our recent studies [28,29], i.e., $(10\bar{1}0)_{Grain2}//(0001)_{Grain2}$ and $[1\bar{2}10]_{Grain1}//[1\bar{2}10]_{Grain2}$. Sample C with a $\{1\bar{2}10\}$ asymmetric tilt grain boundary (ATGB) is created by requiring the crystallographic orientations $(10\bar{1}2)_{Grain2}//(0001)_{Grain2}$ and $[10\bar{1}1]_{Grain1}//[10\bar{1}0]_{Grain2}$.

The interaction between atoms is described by a modified embedded atom method (MEAM) potential with a cubic-spline based functional form [30], and the potential provides a reasonable description of the pressure induced $\alpha \rightarrow \omega$ phase transitions in Ti [31]. Periodic boundary conditions are applied in the x and y directions to mimic the uniaxial strain condition of planar shock loading. Shock waves are generated along the z axis by taking two surface layers at one end of the sample as a reflecting "momentum mirror" or stationary piston and driving the sample towards the mirror at a certain drift velocity. The drift velocity refers to the particle velocity behind the shock wave. The trajectory of each atom

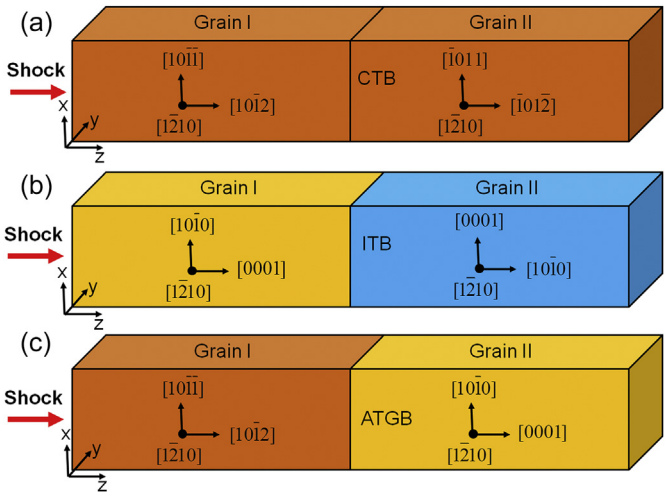

Fig. 1. Schematic configurations of Ti bicrystals with (a) a $\{10\bar{1}2\}_{\alpha}$ coherent twin boundary, CTB (b) an incoherent twin boundary, ITB and (c) $\{1\bar{2}10\}_{\alpha}$ asymmetric tilt grain boundary, ATGB. Shock loading is normal to the interface, and the shock waves (piston velocity, $u_p = 0.8$ km/s) propagate from left to right.

is then integrated by a predicter-corrector scheme with a time step of 1 fs. A bond-angle distribution related order parameter (ADOP) developed by Ackland is utilized to distinguish the different structural phases [32]. Prior to compression, the as-constructed bicrystals are first equilibrated to achieve a minimum energy state using the conjugate gradient method, and then annealed at 30 K for about 100 ps. We choose this low temperature deliberately as our main aim is to study the dislocation activity and martensitic transformation at GBs. Since the temperature increases under loading, a low starting temperature allows us to identify dislocations relatively easily. What's more, the stress (σ_{ij}) and particle velocity (u_{zz}) profiles are extracted from MD simulations via a one-dimensional (1D) binning analysis. For a given simulation geometry, we divide the simulation cell into fine bins along the shock direction, and the average physical properties are obtained within each bin. The center-of-mass velocity of a bin is removed when calculating temperature and stress. Stress for each bin is the averaged virial stress plus thermal contributions.

In addition to MD simulations, *ab initio* calculations using the Vienna *ab initio* simulation package (VASP) [33] were performed to compute the energy barrier for homogeneous hcp-ω transformation in Ti with a generalized solid−state nudged elastic band (G-SSNEB) method [34]. The energy cutoff for the plane-wave basis was set to 400 eV, and a $15 \times 11 \times 11$ k-point was utilized according to the Monkhorst-Pack scheme. The exchange−correlation functional was constructed according to the generalized gradient approximation (GGA) of Perdew Burke Ernzerhof (PBE) [35]. The calculations converged to 10^{-5} eV/cell and the NEB was considered to be complete when the total force on each image of atomic configuration was less than 0.02 eV/Å.

3. Results

3.1. The interaction of shock waves with grain boundaries

Wave profile measurements and their interpretation play a central role in shock physics research. Theoretically, much information about the dynamic material response of Ti bicrystals can be deduced from the wave profiles. The best way to understand the resulting shock wave states is graphically using wave propagation position-time (x-t) diagrams. Therefore, we plot the evolution of

particle velocity (u_{zz}) and the shear stress ($\sigma_v = \sigma_{zz} - (\sigma_{xx} + \sigma_{yy})/2$) in the position-time diagrams, as shown in Fig. 2 and Fig. 3, respectively.

Fig. 2 shows a particle velocity u_P profile for Ti bicrystals in terms of a position-time diagram. The position-time-velocity diagram consists of four regions, i.e., a shocked region (S-region), a transmissive region (T-region), an unshocked region (O-region) and a release region (R-region), respectively. This evolution of u_P is as a result of the incident shock waves I_{GB}, the subsequent interaction of the incident waves with the GBs (which can lead to the formation of transmission wave T_{GB} and reflection wave R_{GB}, see the arrows in Fig. 2), as well as the release fans originating at the free surfaces. It is interesting to note that we observe a sharp particle velocity attenuation (from S-region to T-region in Fig. 2) as the elastic precursor passes through the GB (with a CTB local structure), due to the wave reflection and scattering associated with the GBs.

Our main interest concerns how the GB geometry affects the dynamic response of the Ti bicrystals. The interaction of shock wave with GBs can lead to inelastic deformation (such as dislocation activity and $\alpha \rightarrow \omega$ transformation), giving rise to considerable structure changes and stress relaxation. We compare the difference of shock response among the $u_p = 0.80$ km/s shock-loaded CTB, ITB and ATGB bicrystals, and the results are shown in the shear stress profiles of Fig. 3. As the compression loading is applied, shock waves in the bicrystal samples propagate toward the GB (black dashed lines in Fig. 3) from the left free surface. For the sample containing CTB, the shear stress on both sides of the GB is reduced sharply as the leading elastic shock passes the CTB (at ~8 ps). Further loading gives rise to the interaction of the incident plastic wave (or phase transition wave) with the GB reflected inelastic wave in Grain I ($t > 13$ ps), leading to more shear stress reduction (as shown in the red triangle of in Fig. 3(a)). This indicates two inelastic shock waves (hereafter referred to as two-side GB plasticity), i.e., one reflected shock in the left grain (Grain I) and one transmitted shock in the right grain (Grain II), are triggered when the elastic precursor arrived at CTB. It is important to note that such two-side GB plasticity is triggered by the elastic precursor, not due to the arrival of the plastic shock wave. This is quite different from the shock response of Cu bicrystals, where the CTB region is intact upon the passage of the elastic wave [36].

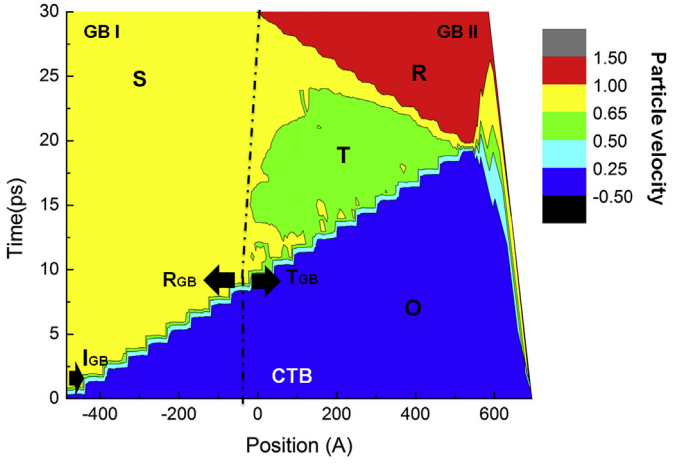

Fig. 2. The position-time-velocity diagram for the CTB bicrystal loaded with piston velocity, $u_p = 0.8$ km/s. The impact plane is at $z = 0$. Color coding is based on particle velocity V_{zz}. Region O: unshocked; S: shocked; T transmitted; R: release. The arrows indicate the shock wave associated with the GB: I_{GB}, T_{GB} and R_{GB} are incident wave, transmission wave and reflection wave, respectively. CTB represents the $\{10\bar{1}2\}_\alpha$ coherent twin boundary, and GB is grain boundary.

In contrast, the other two types of GB structures show a different dynamic response under shock loading, and both cases show an elastic precursor triggered inelastic deformation only on one-side of the GB regions (hereafter referred to as one-sided GB plasticity). As shown in Fig. 3(b), only a transmitted inelastic shock in grain II is induced when the ITB is swept by the elastic precursor at $t \approx 8$ ps, and the shear stress in the ITB region closed to grain I side keeps unchanged before the arrival of the incident plastic shock wave. Fig. 3(c) demonstrates the other type of one-sided GB plasticity in the ATGB region. The interaction of the elastic wave with the ATGB leads to a reflected inelastic shock in grain I, while grain II is unaffected before the incident plastic shock passes the grain boundary.

3.2. Plastic deformation and phase transformation at grain boundaries

In order to understand the difference in the shock response of Ti bicrystals, we studied the deformation mechanisms involved in the elastic-wave triggered GB plasticity. Previous studies on the shock response of nanocrystalline fcc metals have indicated that the occurrence of GBs introduces more complexity in the deformation mechanisms in GB regions, including stacking fault formation, pronounced twinning, dislocation slip and GB sliding [2,16]. By examining multiple snapshots stored during the MD simulations along with relevant parts of the atomic trajectories, we find that three deformation modes, i.e., dislocation slip, GB migration and $\alpha \rightarrow \omega$ phase transformation are involved in the GB plasticity for shock compressed Ti bicrystals with different GBs. The dominant deformation mechanisms are sensitive to the GB geometry.

3.2.1. $\{10\bar{1}2\}$ coherent twin boundaries

Fig. 4 shows the corresponding atomic microstructure evolution of the shock-loaded Ti bicrystal containing a $\{10\bar{1}2\}$ CTB. The Ti atoms are colored according to their local atomic packing determined from characteristic bond angle analysis [32]. Atoms with a hcp environment are shown as orange spheres and represent the α phase, whereas the blue and orange regions mark the ω phase, other colors denote defect atoms. After a drift velocity of $u_p = 0.80$ km/s is applied to a perfect Ti bicrystal sample (Fig. 4(a)), the elastic, plastic as well as phase transformation waves originating at the impact plane begin to propagate toward the CTB, and the $\alpha \rightarrow \omega$ martensitic transformation occurs from the impact plane. Interestingly, we noticed that the $\alpha \rightarrow \omega$ transformation is also triggered at the CTB region when the elastic precursor arrived at CTB (Fig. 4(b)). Further loading leads to the growth of the ω nuclei within the CTB region toward the interior of both grain I and II (Fig. 4(c) and (d)). This process is consistent with the two-sided GB plasticity indicated in the triangular region of Fig. 3(a). Thus, we can summarize that the $\alpha \rightarrow \omega$ transformation contributes significantly to the GB plasticity in CTB bicrystals. Our finding is also consistent with our previous study on shocked Zr polycrystals [18,28], which showed some deformation twinning mediating the $\alpha \rightarrow \omega$ transformation process. In addition, we find that the $\alpha \rightarrow \omega$ transformation process is also accompanied by a complex dislocation activity. As the shock wave propagates toward the CTB, a considerable number of dislocations gliding on the same slip system first nucleate at the plastic shock front (see the green atoms in Fig. 4(b)). As the elastic precursor sweeps past the CTB, some partial dislocations are emitted from the CTB region (Fig. 4(b)). Under further loading, the density of dislocations increases and more than one slip system is activated, giving rise to a more complex dislocation morphology, as shown in Fig. 4(c) and (d).

For a better understanding of dislocation activity in shock compressed Ti CTB bicrystals, we re-examined in detail the

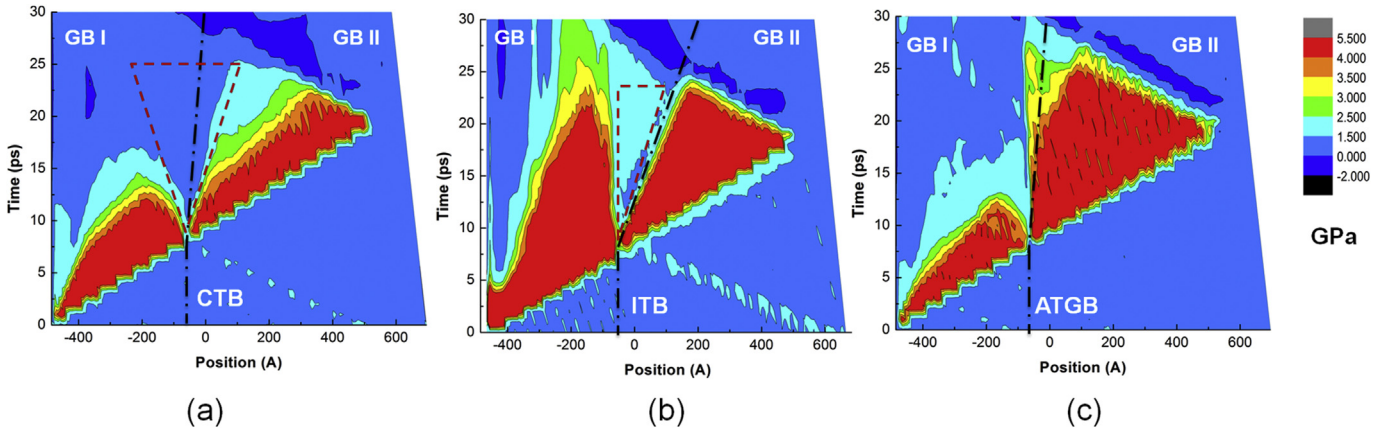

Fig. 3. The position-time-shear stress diagram for the CTB, ITB and ATGB bicrystals shock-loaded with u_p = 0.8 km/s. Color coding is based on the local shear stress ($\sigma_{zz} - (\sigma_{xx} + \sigma_{yy})/2$)). The black dot dash line is the updated grain boundaries position, and the red triangle region shows where elastic wave induced phase transformation occurs. As the leading elastic shock passes the grain boundaries, the shear stress on both sides of the CTB is reduced (a); However, shear stress reduction only occurs in the ITB region closed to grain II side (b), and the shear stress decreases in the ATGB region closed to grain I side (c). Here, CTB, ITB and ATGB are coherent twin boundary, incoherent twin boundary and asymmetric tilt grain boundary, respectively. (For interpretation of the references to colour in this figure legend, the reader is referred to the web version of this article.)

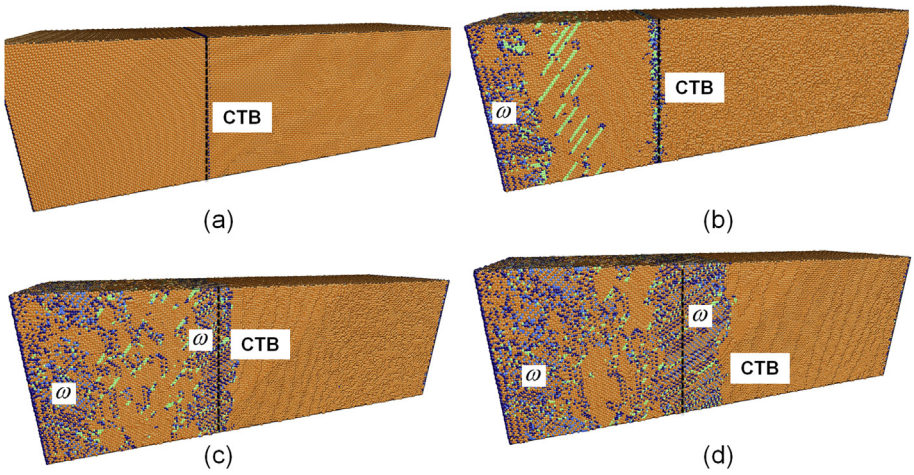

Fig. 4. Snapshots of the CTB response to the elastic, plastic and phase transition shocks with a piston velocity of u_p = 0.80 km/s. When the shock wave is applied to a perfect Ti bicrystal (a), basal dislocations are formed at the incident plastic wave front, and ω phase also nucleate at the CTB upon passage of the elastic precursor (b). Under further loading, ω phase in the CTB region continues to grow, accompanied by the formation of a complex dislocation morphology ((c) and (d)). The orange and orange-and-blue regions represent the hcp α phase and the hex ω phase, respectively. The atoms belong to partial and full dislocations are colored by green and dark blue, respectively. CTB represents the $\{10\bar{1}2\}_\alpha$ coherent twin boundary. (For interpretation of the references to colour in this figure legend, the reader is referred to the web version of this article.)

dislocation glide process by a direct atomic configuration analysis. The plastic deformation of hcp metals is dominated by the movement of $\langle \vec{a} \rangle$ dislocations with the shortest Burgers vector: $\langle 1\bar{2}10 \rangle$. In quasi-static deformed α-Ti, the easiest slip mode is prismatic $\{10\bar{1}0\}$ $\langle 1\bar{2}10 \rangle$, and the basal slip and the first order pyramidal slip operate as the less prominent slip modes [7,37], inidcated as P, B and π in Fig. 5(a), repectively. Fig. 5(b) shows a snapshot of shock compression-induced deformation microstructure at 10 ps, especially the dislocation morphology within the CTB bicrystal. We find that $\langle \vec{a} \rangle$ dislocations gliding in basal planes are first generated as the incident plastic wave penetrates into the material. This is in agreement with the results of recent measurements on Zr [38], which show that anomalous basal slip activity dominates the plasticity under high strain rate. At the same time, a considerable number of basal partial dislocations (brown color) are emitted from the CTB region due to the elastic precursor. With the advancing shock front, the basal dislocations emitted from the CTB interact with the basal dislocations nucleated at the incident plastic wave front (Fig. 5(c)), giving rise to the operation of pyramidal slip (π in Fig. 5(d)). When the whole sample is shocked (18 ps), the dislocation morphology consists mainly of $\langle \vec{a} \rangle$ dislocations gliding in the pyramidal plane (π in Fig. 5(e), yellow color). And a small amount of prismatic glide (P, green color) is also observed in the plastic deformed region. These results demonstrate the significant effect of CTBs on changing dislocation slip systems in shocked α-Ti.

3.2.2. *Incoherent twin boundaries*

The incoherent twin boundary (ITB) is another GB equilibrium structure within hcp-Ti, which can be decomposed into several CTB segments connected by $\langle \mathbf{a} + \mathbf{c} \rangle$ dislocations. Recent investigation reveals that the migration of ITB also plays an important role in accommodating the plasticity of hcp metals undergoing extreme compression [28,39]. Fig. 6 shows the atomic details of a Ti bicrystal with ITB for different deformation stages under u_p = 0.80 km/s shock compression. When deformation occurs, only an α → ω martensitic transformation process is triggered from the impact plane, and no dislocation activity was observed, as shown in Fig. 6(b). In addition, a wavy GB is formed during the passing of the

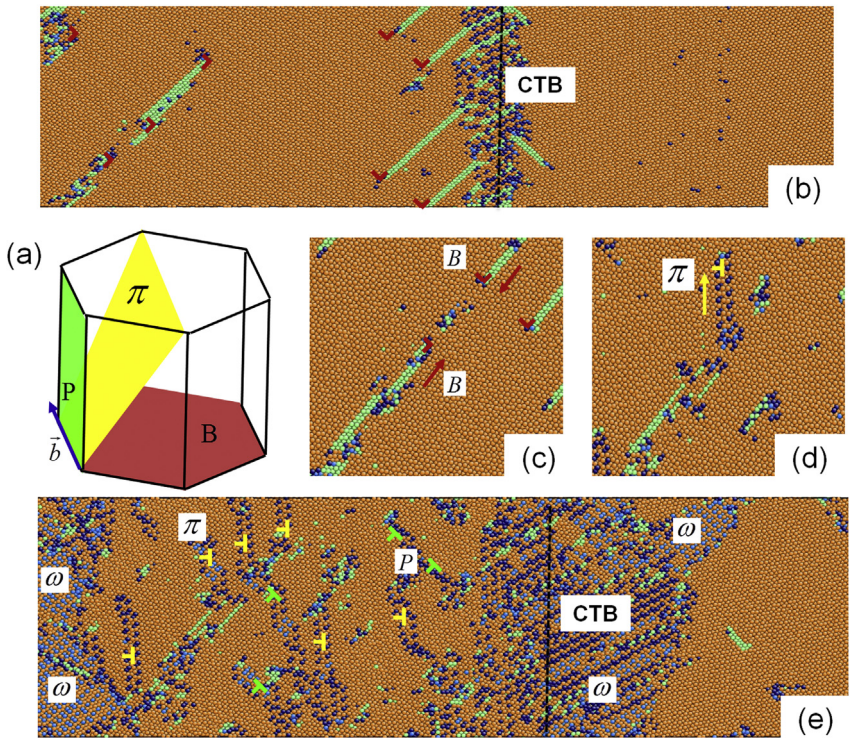

Fig. 5. Dislocation mediated plasticity at a CTB in Ti bicrystal shock-loaded at $u_p = 0.8$ km/s. (a) Sketch of $\langle \vec{a} \rangle$ dislocation glide planes in α-Ti. As the compression loading is applied, a considerable number of basal dislocations are emitted from the CTB (b). These dislocations interact with the basal dislocations nucleated at the incident plastic wave front (c), forming pyramidal dislocations (d). As a result, a pyramidal dislocations dominated morphology is formed after 18.0 ps (e). The orange and orange-and-blue regions represent the hcp α phase and the hex ω phase, respectively. The symbols colored brown, yellow and green show the dislocations gliding in the basal (B), pyramidal (P) and prismatic (π) planes, respectively. CTB represents the $\{10\bar{1}2\}_\alpha$ coherent twin boundary. (For interpretation of the references to colour in this figure legend, the reader is referred to the web version of this article.)

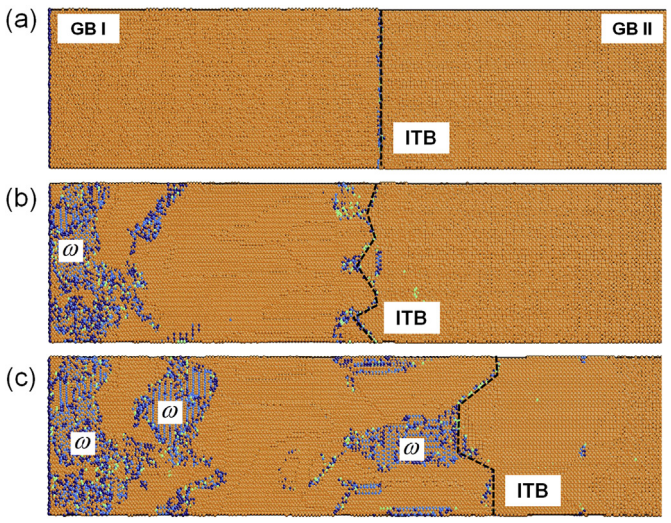

Fig. 6. The microstructure evolution of the ITB bicrystal response to shock compression with $u_p = 0.8$ km/s. When a perfect ITB bicrystal (a) is shock compressed, the passing of the elastic precursor leads to the ITB moving along the shock direction (b), preceding the $\alpha - \omega$ phase transformation process (c). The orange and the light blue (also blue stacking) colors represent the hcp α phase and the hex ω phase, respectively. ITB represents the incoherent twin boundary. (For interpretation of the references to colour in this figure legend, the reader is referred to the web version of this article.)

elastic precursor (Fig. 6(b)). As the shock front advances, the grain I begins to grow at the expense of grain II, and a trapezoidal GB structure is formed, as shown in Fig. 6(c). This indicates the occurrence of the shock compression driven 90° GB motion. Our previous work suggests that this boundary migration process is via a transformation-like lattice reorientation accompanied by a collective action of dislocations and deformation twins. In addition, a considerable volume fraction of precipitated ω phase is observed in the lattice regions left by the moving GB, indicating strong coupling between the GB motion and the $\alpha \rightarrow \omega$ martensitic transformation. It is quite different from the CTB case, where the ω phase directly nucleated from the CTB region. Such coupling mechanism associated with the ITB is the response to the one-sided shear stress reduction shown in the triangular region of Fig. 3(b).

3.2.3. *Asymmetric tilt grain boundary* $\{1\bar{2}10\}$

Fig. 7 shows the different deformation stages for a Ti bicrystal under shock with an $\{1\bar{2}10\}$ asymmetric tilt grain boundary (ATGB). As shown in Fig. 7(a), the equilibrium structure of the ATGB shows a plane with a certain interface roughness, which can facilitate dislocation nucleation in later GB deformation stages. Upon shock compression, both the $\alpha \rightarrow \omega$ martensitic transformation and dislocation glide occurs in the region swept by the plastic shock (Fig. 7(b)), and basal partial dislocations in the GB region are nucleated and emitted continuously into grain I due to the elastic shock wave. The interaction between these basal partial dislocations leads to the formation of pyramidal glide dominated dislocation morphology (Fig. 7(c)). We note that the dislocation activity occurs only in Grain I but not in Grain II, which coincides with the one-sided GB plasticity inferred from Fig. 3(d). This phenomenon can be attributed to the asymmetric GB with different orientation angles in the two lattices, and the nucleation of dislocations in the grain with low orientation angle is energetically preferable. The

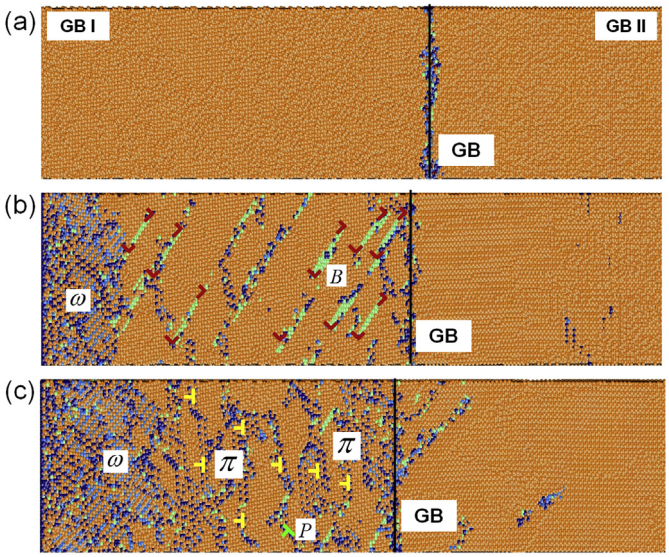

Fig. 7. The microstructure evolution of the ATGB bicrystal response to shock compression with u_p = 0.8 km/s. The initial configuration (a) is a perfect ATGB bicrystal. The propagation of the elastic, plastic and phase transition shock front leads to the formation of a high density of pyramidal dislocations as well as the growth of ω phase ((b) and (c)). The orange and orange-and-blue regions represent the hcp α phase and the hex ω phase, respectively. The symbols colored brown, yellow and green show the dislocations gliding in the basal (B), pyramidal (P) and prismatic (π) planes, respectively. ATGB represents the $\{1\bar{2}10\}_\alpha$ asymmetric tilt grain boundary, and GB is grain boundary. (For interpretation of the references to colour in this figure legend, the reader is referred to the web version of this article.)

propagation of the shock front then leads to the formation of a high density of pyramidal dislocations as well as the growth of ω phase (Fig. 7(c)). It is interesting to note that the ATGB is almost intact during the passage of the elastic wave and the plastic shock only induces minor GB structural changes.

3.3. *Effect of coherent twin boundaries (CTB) on shock wave damping*

Another interesting phenomenon accompanied by the unique structural features in CTB regions is the strong elastic shockwave decay. We then studied the corresponding stress profiles in Ti CTB bicrystals. Fig. 8 shows the evolution of lateral stress σ_{yy} for a CTB bicrystal shock-loaded with up = 0.80 km/s (σ_{yy} is most illustrative amongst σ_{xx}, σ_{yy}, and σ_{zz} as regards wave features). It is shown that the elastic precursor induces GB plasticity accompanied by a decay in the elastic-wave amplitude when crossing the CTB. A GB-induced phase transformation wave plateau develops (from 12 ps to 15 ps in Fig. 8). The elastic wave decay is due to the α → ω martensitic transformation in the GB region triggered by the elastic shock (Fig. 4). However, the plastic shock wave initiated from the impact plane first interacts with the elastic-precursor-induced plastic wave as well as phase transformation wave in Grain I (12 ps). It then arrives at the CTB and passes through it and further interacts with the GB phase transformation in Grain II (15 ps). During these interactions, the strength of the plastic shock wave is also reduced (18 ps). Thus, a five-wave structure is formed across the CTB, including the transmitted elastic shock, GB phase transformation shock, transmitted plastic shock, plastic shock, and phase transformation shock marked in Fig. 8 at 18 ps by numbers 1–5. Although the five-wave features cannot be obtained directly from the longitudinal stress σ_{zz} profile, the decay in σ_{zz} has also been observed as the elastic wave sweeps past the CTB, as shown in Fig. 9.

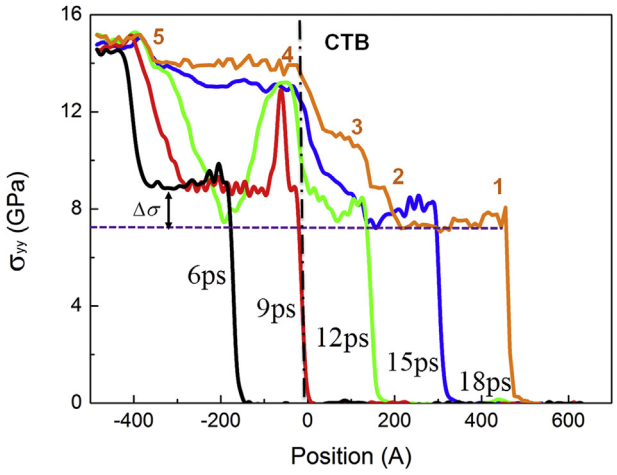

Fig. 8. Evolution of the lateral stress σ_{yy} wave profiles for the CTB bicrystal shock-loaded with u_p = 0.8 km/s. The initial position of the CTB is marked with a black dashed line. The interaction of the elastic wave with the CTB gives rise to considerable stress attenuation $\Delta\sigma_{yy}$. CTB represents the $\{10\bar{1}2\}_\alpha$ coherent twin boundary.

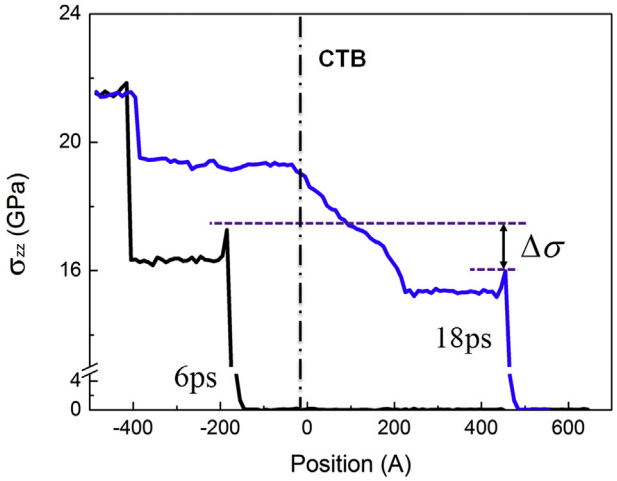

Fig. 9. The longitudinal pressure σ_{zz} decay associated with CTB in the Ti bicrystal sample shock-loaded with u_p = 0.8 km/s. CTB is the $\{10\bar{1}2\}_\alpha$ coherent twin boundary.

The shock wave decay in the longitudinal and lateral stress profiles indicates that the $\{10\bar{1}2\}$ CTB can modulate shock waves via the GB triggered α → ω phase transformation, giving rise to considerable wave attenuation or shock damping. In order to confirm this damping effect, we further investigated with simulations the damping efficiency of CTBs of a model Ti polycrystal containing 40 CTBs (up to 0.5 μm). Fig. 10(a) shows the evolution of the σ_{zz} stress profiles as a function of time, and the rapid decay of the elastic precursor can be readily identified. We quantify the elastic shock strength as a function of propagation distance at different times (Fig. 10(b)), and find that σ_{zz} decreases from an initial value of 19.6 to 12.3 GPa after the elastic precursor traverses 40 CTBs, corresponding to an elastic shock decay of ~40%. Fig. 10(c) shows the corresponding atomic microstructure located near the free-surface end (after considerable decay), and considerable ω phase is observed in the CTB regions. Previous studies usually attribute the elastic precursor decay to the dislocation activity mediated stress relaxation behind elastic shock front. Our MD simulation results indicate that the CTB-induced phase transformation is another effective decay mechanism, and this unique

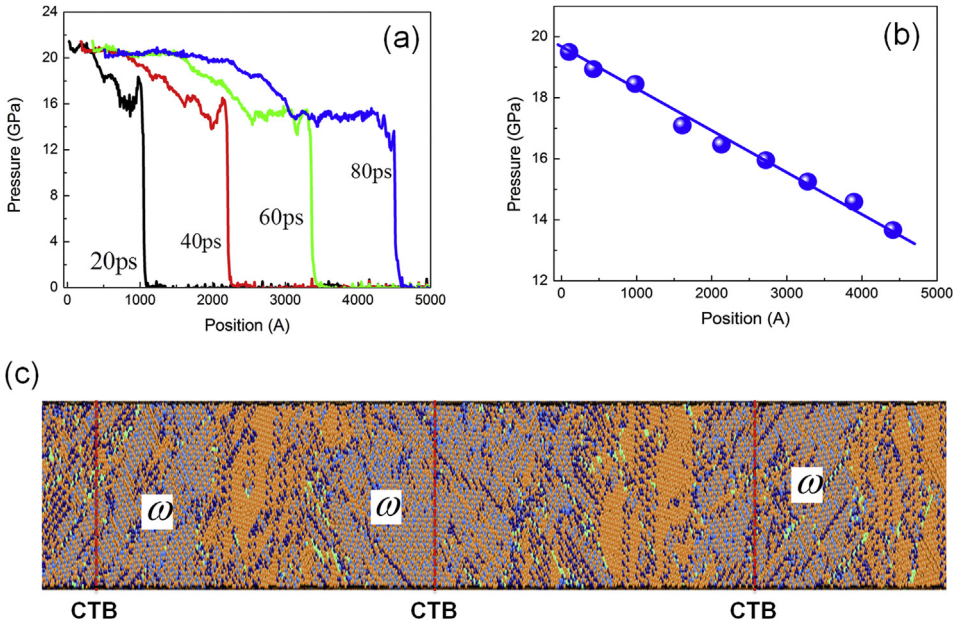

Fig. 10. Shock response of a Ti sample containing many CTBs shock-loaded with $u_p = 0.8$ km/s. (a) The longitudinal pressure σ_{zz} profiles of the multi-CTBs Ti sample for t = 20 ps, 40 ps, 60 ps and 80 ps, respectively. (b) The elastic precursor decay due to multi-CTBs plasticity. The position refers to the elastic shock front position during its propagation. (c) Atomic configuration of the multi-CTBs Ti sample for t = 80 ps near the target end. CTB represents the $\{10\bar{1}2\}_\alpha$ coherent twin boundary.

feature can potentially be used for designing new types of shock-damping materials.

4. Discussion

Simulations on shock compressed Ti bicrystals reveal that $\{10\bar{1}2\}$ CTBs can promote α → ω martensitic transformation, and ω phase can even be triggered by the elastic precursor (Fig. 4). In contrast, grain boundary induced phase transformation does not occur in the other two types of bicrystals containing an ITB or ATGB. Our discussion below emphasizes that the unique shock response of $\{10\bar{1}2\}$ CTBs stems from its intermediate-state-like local atomic packing.

4.1. Crystallographic modeling of CTB assisted α → ω transformation

Crystallographically, the martensitic transformation process can be expressed as the result of the coupled effects of shear strains and shuffles (or atomic displacements). Fig. 10(a) shows the atomic configurations containing both parent phase and product phase in a shocked Ti bicrystal, which shows an atomic stacking rearrangement from $(1\bar{2}10)_\alpha$ (black tetragon in Fig. 11(a)) to $(01\bar{1}1)_\omega$ (red tetragon) during the α → ω transformation process. We suggest that the $(01\bar{1}1)_\omega$ stacking can be obtained by shifting two inner atom shuffles in opposite directions (shown by arrows in Fig. 11(c)), facilitated by the presence of $\{10\bar{1}2\}$ CTBs. As shown in Fig. 11 (c), the atomic stackings of $(1\bar{2}10)_\alpha$ and $(01\bar{1}1)_\omega$ are compared with the corresponding local packing of the CTBs, which is selected from the $\{10\bar{1}2\}$ CTB regions (blue tetragon in Fig. 11(b)). It can be seen that the inner-atom shuffle is reduced with the assistance of the $\{10\bar{1}2\}$ CTBs. In addition, we calculated the radial distribution function (RDF) of the relevant local structures (Fig. 11(d)); the RDF of the $\{10\bar{1}2\}$ CTB regions has the characteristics of both α phase and ω phase indicating that the $\{10\bar{1}2\}$ CTB has an intermediate structure of α phase and ω phase. Therefore, in a α-Ti bicrystal containing $\{10\bar{1}2\}$ CTBs, the ω phase nucleating in the $\{10\bar{1}2\}$ CTB region is not only feasible but also easier than nucleating directly in the α matrix.

4.2. Role of CTBs in overcoming the energy barrier of the α→ω transformation

The kinetics of martensitic transformation are often associated with the transformation pathways or mechanisms as these determine the nucleation barrier for a martensitic embryo. There are two commonly observed direct (without intermediate structures) transformation pathways in Zr, Ti for the α → ω transformation, namely, Silcock [40] and TAO-1 [41]. In order to determine the phase transformation mechanism, we examined the relative orientation of coexisting phases in shocked specimens. An image of an oriented thin section of the shocked CTB specimen with indices of the parallel crystallographic planes is shown in Fig. 11(a). The orientation relationship observed here was identified as follows: $(0001)_\alpha // (10\bar{1}1)_\omega$ and $[10\bar{1}0]_\alpha // [\bar{1}011]_\omega$ or TAO-1 pathway, which is consistent with the mechanics of the transformation observed by Song and Gray for Zr [42].

In order to probe the underlying mechanism for the connection between $\{10\bar{1}2\}$ CTBs and the α → ω phase transformation kinetics, *ab initio* calculations were performed to determine the energy landscape along the TAO-1 pathway. During the calculations, the lattice parameters of each crystal structure were optimized to minimize the total energy. The change of the chemical energies with respect to the hcp structure of α phase for each intermediate structure is shown in Fig. 12(a). According to the energy landscape along the TAO-1 pathway (Fig. 12(a)), if there is a local shear strain or shuffle rearranging the atoms to the metastable structure shown by the arrow in Fig. 12(a), the energy barrier will be overcome and the transition can then occur more easily. Thus, the atomic rearrangement provides assistance. Indeed, the local atomic configurations along the $\{10\bar{1}2\}$ CTB are similar to the TAO-1 metastable structure shown by the arrow in Fig. 12(a). As shown in Fig. 12(b), the RDFs of both the TAO-1 metastable structure and the $\{10\bar{1}2\}$ CTB are similar, i.e., the calculated positions of the first three peaks

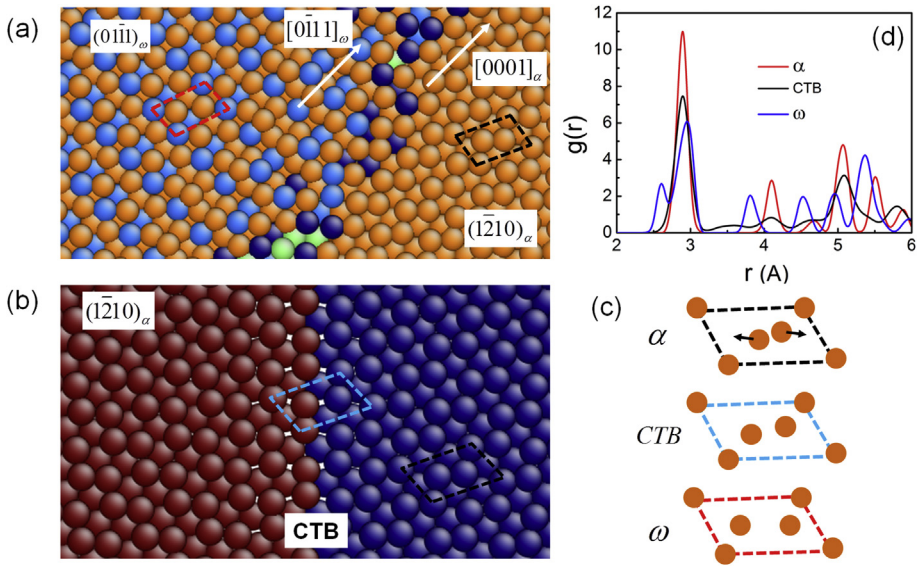

Fig. 11. Comparison of local structure in α phase, ω phase and CTBs. (a) Microstructure showing the orientation relationship between the α phase and transformed ω phase, indicating a TAO-1 pathway. (b) Local atomic configuration for a perfect CTB. (c) The corresponding atom stacking of $(0\bar{1}11)_\omega$, $(1\bar{2}10)_\alpha$ and CTB planes. The arrows point in the shuffle direction. (d) The radial distribution functions for α, ω and the local structure of CTBs. Here, CTB is the $\{10\bar{1}2\}_\alpha$ coherent twin boundary.

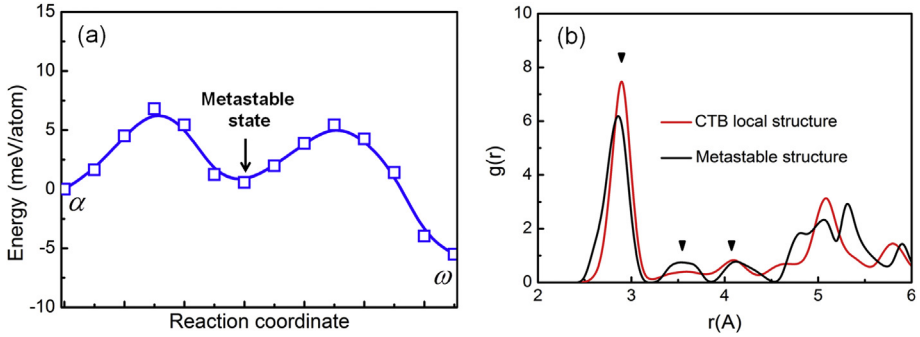

Fig. 12. Similarity between CTB local structure and the metastable structure mediated the α − ω phase transformation. (a) Change of potential energy during the α − ω phase transformation according to TAO-1 pathway, which involves a metastable state. (b) Comparison of the radial distribution functions between CTB and metastable structure shown in (a). CTB represents the $\{10\bar{1}2\}_\alpha$ coherent twin boundary.

in both cases are coincident. This indicates that $\{10\bar{1}2\}$ CTBs assist in overcoming the energy barrier for the α → ω transition pathway, and explains why the α → ω phase transformation in the $\{10\bar{1}2\}$ CTB regions can occur at a much lower pressure, i.e., the elastic wave readily can trigger the α → ω phase transformation (see Fig. 4).

5. Conclusion

The influence of grain boundaries on phase transformation in Ti under shock compression is investigated via a combination of MD simulations and first principle calculations. We draw the following conclusions: (1) Simulations of shock compressed Ti bicrystals show drastically different shock response (plastic deformation and martenstic transformation) in the presence of GB structures. We find that the elastic shock wave can readily trigger α → ω transformation in $\{10\bar{1}2\}$ CTB bicrystals, and an elastic wave driven grain boundary migration is observed in ITB bicrystals. However, the $\{10\bar{1}2\}$ ATGB is almost intact during the passage of the elastic wave. (2) The dislocation activity in shocked Ti bicrystals with a CTB or ATGB is dominated by the movement of $\langle\vec{a}\rangle$ dislocations. The $\langle\vec{a}\rangle$ dislocations gliding in basal planes are first generated at both the GB and incident plastic wave front, and their subsequent interaction leads to the operation of pyramidal slip. (3) The CTB assisted α → ω phase transformation is accompanied by strong elastic wave attenuation, which can be used for designing new types of shock-damping materials. Although the observations presented and the associated conclusions are based on hcp-Ti, we believe that the coupling between deformation twinning and phase transformation should also apply to other hexagonally transforming metals.

Acknowledgments

This work was supported by the US DOE at LANL (DE-AC52-06NA25396) as well as by the National Natural Science Foundation of China (51320105014, 51321003 and 51501141), the China Postdoctoral Science Foundation (2015M580843), and the 973 Program of China (2012CB619402).

References

[1] M.A. Meyers, H. Jarmakani, E.M. Bringa, B.A. Remington, Chapter 89 dislocations in shock compression and release, in: J.P. Hirth, L. Kubin (Eds.), Dislocations in Solids, vol. 15, Elsevier, 2009, pp. 91–197.

[2] S.J. Fensin, J.P. Escobedo-Diaz, C. Brandl, E.K. Cerreta, G.T. Gray Iii, T.C. Germann, S.M. Valone, Effect of loading direction on grain boundary failure under shock loading, Acta Mater. 64 (2014) 113–122.
[3] H.E. Lorenzana, J.F. Belak, K.S. Bradley, E.M. Bringa, K.S. Budil, J.U. Cazamias, B. El-Dasher, J.A. Hawreliak, J. Hessler, K. Kadau, D.H. Kalantar, J.M. McNaney, D. Milathianaki, K. Rosolankova, D.C. Swift, M. Taravillo, T.W. Van Buuren, J.S. Wark, T.D. de la Rubia, Shocked materials at the intersection of experiment and simulation, Sci. Model. Simul. 15 (2008) 159–186.
[4] J.R. Asay, The use of shock-structure methods for evaluating high-pressure material properties, Int. J. Impact Eng. 20 (1997) 27–61.
[5] N.K. Bourne, G.T. Gray III, J.C.F. Millett, On the shock response of cubic metals, J. Appl. Phys. 106 (2009) 091301.
[6] K. Wang, W. Zhu, S. Xiao, K. Chen, H. Deng, W. Hu, Coupling between plasticity and phase transition of polycrystalline iron under shock compressions, Int. J. Plast. 71 (2015) 218–236.
[7] P.J. Hazell, G.J. Appleby-Thomas, E. Wielewski, J.P. Escobedo, The shock and spall response of three industrially important hexagonal close-packed metals: magnesium, titanium and zirconium, Philos. Trans. R. Soc. A 372 (2014) 2023.
[8] T. Gorkaya, K.D. Molodov, D.A. Molodov, G. Gottstein, Concurrent grain boundary motion and grain rotation under an applied stress, Acta Mater. 59 (2011) 5674–5680.
[9] J.W. Cahn, Y. Mishin, A. Suzuki, Coupling grain boundary motion to shear deformation, Acta Mater. 54 (2006) 4953–4975.
[10] L. Wang, J. Teng, P. Liu, A. Hirata, E. Ma, Z. Zhang, M. Chen, X. Han, Grain rotation mediated by grain boundary dislocations in nanocrystalline platinum, Nat. Commun. 5 (2014) 4402.
[11] H.A. Khater, A. Serra, R.C. Pond, J.P. Hirth, The disconnection mechanism of coupled migration and shear at grain boundaries, Acta Mater. 60 (2012) 2007–2020.
[12] N. Hansen, Hall–Petch relation and boundary strengthening, Scr. Mater. 51 (2004) 801–806.
[13] M.W. Chen, J.W. McCauley, D.P. Dandekar, N.K. Bourne, Dynamic plasticity and failure of high-purity alumina under shock loading, Nat. Mater. 5 (2006) 614–618.
[14] J.A. Hawreliak, B. El-Dasher, H. Lorenzana, G. Kimminau, A. Higginbotham, B. Nagler, S.M. Vinko, W.J. Murphy, T. Whitcher, J.S. Wark, S. Rothman, N. Park, In situ x-ray diffraction measurements of the c/a ratio in the high-pressure epsilon phase of shock-compressed polycrystalline iron, Phys. Rev. B 83 (2011) 144114.
[15] N. Gunkelmann, E.M. Bringa, D.R. Tramontina, C.J. Ruestes, M.J. Suggit, A. Higginbotham, J.S. Wark, H.M. Urbassek, Shock waves in polycrystalline iron: plasticity and phase transitions, Phys. Rev. B 89 (2014) 140102.
[16] E.M. Bringa, A. Caro, Y.M. Wang, M. Victoria, J.M. McNaney, B.A. Remington, R.F. Smith, B.R. Torralva, H. Van Swygenhoven, Ultrahigh strength in nanocrystalline materials under shock loading, Science 309 (2005) 1838–1841.
[17] G.I. Kanel, Spall fracture: methodological aspects, mechanisms and governing factors, Int. J. Fract. 163 (2010) 173–191.
[18] E.K. Cerreta, J.P. Escobedo, P.A. Rigg, C.P. Trujillo, D.W. Brown, T.A. Sisneros, B. Clausen, M.F. Lopez, T. Lookman, C.A. Bronkhorst, F.L. Addessio, The influence of phase and substructural evolution during dynamic loading on subsequent mechanical properties of zirconium, Acta Mater. 61 (2013) 7712–7719.
[19] D.P. Dandekar, Loss of shear-strength in polycrystalline tungsten under shock compression, J. Appl. Phys. 47 (1976) 4703–4705.
[20] R.A. Lebensohn, J.P. Escobedo, E.K. Cerreta, D. Dennis-Koller, C.A. Bronkhorst, J.F. Bingert, Modeling void growth in polycrystalline materials, Acta Mater. 61 (2013) 6918–6932.
[21] P.J. Imrich, C. Kirchlechner, C. Motz, G. Dehm, Differences in deformation behavior of bicrystalline Cu micropillars containing a twin boundary or a large-angle grain boundary, Acta Mater. 73 (2014) 240–250.
[22] T.J. Rupert, D.S. Gianola, Y. Gan, K.J. Hemker, Experimental observations of stress-driven grain boundary migration, Science 326 (2009) 1686–1690.
[23] H. Zong, X. Ding, T. Lookman, J. Li, J. Sun, Uniaxial stress-driven coupled grain boundary motion in hexagonal close-packed metals: a molecular dynamics study, Acta Mater. 82 (2015) 295–303.
[24] S.E. Babcock, R.W. Balluffi, Grain boundary kinetics—II. In situ observations of the role of grain boundary dislocations in high-angle boundary migration, Acta Metall. 37 (1989) 2367–2376.
[25] K. Lu, L. Lu, S. Suresh, Strengthening materials by engineering coherent internal boundaries at the nanoscale, Science 324 (2009) 349–352.
[26] T. Zhu, J. Li, Ultra-strength materials, Prog. Mater. Sci. 55 (2010) 710–757.
[27] S. Plimpton, Fast parallel algorithms for short-range molecular-dynamics, J. Comput. Phys. 117 (1995) 1–19.
[28] H. Zong, X. Ding, T. Lookman, J. Li, J. Sun, E.K. Cerreta, A.P. Escobedo, F.L. Addessio, C.A. Bronkhorst, Collective nature of plasticity in mediating phase transformation under shock compression, Phys. Rev. B 89 (2014) 220101.
[29] H. Zong, T. Lookman, X. Ding, S.-N. Luo, J. Sun, Anisotropic shock response of titanium: reorientation and transformation mechanisms, Acta Mater. 65 (2014) 10–18.
[30] T.J. Lenosky, B. Sadigh, E. Alonso, V.V. Bulatov, T.D. de la Rubia, J. Kim, A.F. Voter, J.D. Kress, Highly optimized empirical potential model of silicon, Model. Simul. Mater. Sci. Eng. 8 (2000) 825–841.
[31] R.G. Hennig, T.J. Lenosky, D.R. Trinkle, S.P. Rudin, J.W. Wilkins, Classical potential describes martensitic phase transformations between the α, β, and ω titanium phases, Phys. Rev. B 78 (2008) 054121.
[32] G.J. Ackland, A.P. Jones, Applications of local crystal structure measures in experiment and simulation, Phys. Rev. B 73 (2006) 054104.
[33] G. Kresse, J. Furthmüller, Efficient iterative schemes for ab initio total-energy calculations using a plane-wave basis set, Phys. Rev. B 54 (1996) 11169–11186.
[34] D. Sheppard, P. Xiao, W. Chemelewski, D.D. Johnson, G. Henkelman, A generalized solid-state nudged elastic band method, J. Chem. Phys. 136 (2012) 074103.
[35] J.P. Perdew, J.A. Chevary, S.H. Vosko, K.A. Jackson, M.R. Pederson, D.J. Singh, C. Fiolhais, Atoms, molecules, solids, and surfaces: applications of the generalized gradient approximation for exchange and correlation, Phys. Rev. B 46 (1992) 6671–6687.
[36] S. Han, L. Zhao, Q. Jiang, J. Lian, Deformation-induced localized solid-state amorphization in nanocrystalline nickel, Sci. Rep. 2 (2012) 493.
[37] E. Clouet, D. Caillard, N. Chaari, F. Onimus, D. Rodney, Dislocation locking versus easy glide in titanium and zirconium, Nat. Mater. 14 (2015) 931–936.
[38] M. Knezevic, I.J. Beyerlein, T. Nizolek, N.A. Mara, T.M. Pollock, Anomalous basal slip activity in zirconium under high-strain deformation, Mater. Res. Lett. 1 (2013) 133–140.
[39] B.Y. Liu, J. Wang, B. Li, L. Lu, X.-Y. Zhang, Z.W. Shan, J. Li, C.L. Jia, J. Sun, E. Ma, Twinning-like lattice reorientation without a crystallographic twinning plane, Nat. Commun. 5 (2014) 3297.
[40] H.R. Wenk, P. Kaercher, W. Kanitpanyacharoen, E. Zepeda-Alarcon, Y. Wang, Orientation relations during the α-ω phase transition of zirconium: in situ texture observations at high pressure and temperature, Phys. Rev. Lett. 111 (2013) 195701.
[41] D.R. Trinkle, R.G. Hennig, S.G. Srinivasan, D.M. Hatch, M.D. Jones, H.T. Stokes, R.C. Albers, J.W. Wilkins, New mechanism for the α to ω martensitic transformation in pure titanium, Phys. Rev. Lett. 91 (2003) 02570.
[42] S.G. Song, G.T. Gray, Microscopic and crystallographic aspects of retained ω-phase in shock-loaded zirconium and its formation mechanism, Philos. Mag. A 71 (1995) 275–290.